Earth and Planetary Science Letters 403 (2014) 432–445

Contents lists available at ScienceDirect

Earth and Planetary Science Letters

www.elsevier.com/locate/epsl

Snap, Crackle, Pop: Dilational fault breccias record seismic slip below the brittle–plastic transition

Ben L. Melosh [a,*], Christie D. Rowe [a,b], Louis Smit [b], Conrad Groenewald [c,d], Christopher W. Lambert [c,d], Paul Macey [c]

[a] Department of Earth and Planetary Sciences, McGill University, Montréal, QC, H3A 0E8, Canada
[b] Department of Geological Sciences, University of Cape Town, Private Bag X3, Rondebosch, 7701, South Africa
[c] Council for Geoscience, 3 Oos Street, Bellville, 7530, South Africa
[d] Department of Earth Sciences, Stellenbosch University, Private Bag X1, Matieland, 7602, South Africa

ARTICLE INFO

Article history:
Received 3 February 2014
Received in revised form 30 June 2014
Accepted 3 July 2014
Available online 7 August 2014
Editor: P. Shearer

Keywords:
dilational fault breccia
earthquake
dynamic fracture
brittle–plastic transition
particle size distribution
paleoseismic tool

ABSTRACT

Off-fault dynamic tensile cracks form behind an earthquake rupture front with distinct orientation and spacing. These cracks explode the wall rock and create breccias, which we hypothesize will preserve a unique fingerprint of dynamic rupture. Identification of these characteristic breccias may enable a new tool for identifying paleoseismic slip surfaces in the rock record. Using previous experimental and theoretical predictions, we develop a field-based model of dynamic dilational breccia formation. Experimental studies find that secondary tensile fracture networks comprise closely spaced fractures at angles of 70–90° from a slip surface, as well as fractures that branch at angles of ~30° from a primary mode I fracture. The Pofadder Shear Zone, in Namibia and South Africa, preserves breccias formed in the brittle–ductile transition zone displaying fracture patterns consistent with those described above. Fracture spacing is approximately two orders of magnitude less than predicted by quasi-static models. Breccias are clast-supported, monomict and can display an abrupt transition from fracture network crackle breccia to mosaic breccia textures. Brecciation occurs by the intersection of off-fault dynamic fractures and wall rock fabric; this is in contrast to previous models of fluid pressure gradient-driven failure "implosion breccias". This mechanism tends to form many similar sized clasts with particle size distributions that may not display self-similarity; where self-similarity is observed the distributions have relatively low D-values of 1.47 ± 0.37, similar to other studies of dynamic processes. We measure slip distances at dilational breccia stepovers, estimating earthquake magnitudes between M_w 2.8–5.8 and associated rupture lengths of 0.023–3.3 km. The small calculated rupture dimensions, in combination with our geologic observations, suggest that some earthquakes nucleated within the quartz-plastic transitional zone and potentially record deep seismic slip.

1. Introduction

Continental scale, strike-slip fault systems define the boundaries of continental plates or micro-plates, accommodate large amounts of displacement (Sylvester, 1988), and host large earthquakes that can reach up to ~M 8 (Lin et al., 2002; Stirling et al., 2007). The nucleation and cessation of fault ruptures are in part controlled by deformation mechanisms operating during the seismic cycle (Tse and Rice, 1986; Scholz, 1998, 2002; Rice, 2006). Within the seismogenic zone where velocity weakening mechanisms dominate, an increase in slip rate causes a strength reduction on the fault plane allowing for large earthquakes to occur (Sibson, 1977; Scholz, 1988, 1998, 2002). This is manifested by the concentration of earthquakes between approximately 5–15 km depth (Sibson, 1984). However, earthquake rupture is not limited to the seismogenic zone and can propagate into velocity strengthening regimes due to the strain rate sensitivity of deformation mechanisms (Sibson, 1983; Scholz, 1988). The lower boundary of the seismogenic zone in granitic crust is defined by the onset of quartz plasticity marking the top of a quasi-plastic transitional zone (Sibson, 1980; Scholz, 1988).

The study of ancient exhumed faults (e.g. Sibson, 1977) or actively exhuming faults (e.g. Toy et al., 2008) presents an opportunity to study deformation mechanisms operating at seismogenic or sub-seismogenic depths. The most widely accepted evidence of earthquakes in exhumed faults is tectonically generated

* Corresponding author. Tel.: +1 514 398 6767, fax: +1 514 398 4680.
E-mail address: benjamin.melosh@mail.mcgill.ca (B.L. Melosh).

http://dx.doi.org/10.1016/j.epsl.2014.07.002
0012-821X/

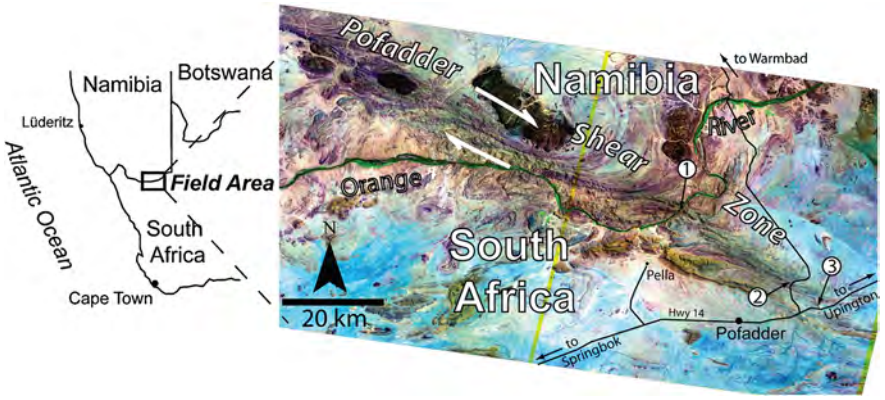

Fig. 1. Location of field area in southern Africa, and a false color ASTER (USGS and Japan ASTER Program, 2013) scene showing the Pofadder Shear Zone and focus locations Coboop (1), Kabas (2), and Pofadder East (3).

psuedotachylyte (Sibson et al., 1975; Sibson, 1989; Cowan, 1999), but this is not the only record. Other features indicative of paleoseismicity that are visible in the field include off-fault injection veins of fault gouge or cataclasite (Lin, 1996, 2011; Rowe et al., 2012).

1.1. Dilational implosion breccias

Earthquake rupture is governed, in part, by fault geometry, particularly at releasing step-overs (Harris et al., 1991), which can often host dilational breccias. Such breccias have been hypothesized to form seismically resulting from wall rock implosion (Sibson, 1985, 1986), making them important paleo-earthquake markers, but also creating sites of maximum coseismic dilation responsible for fluid transport and ore deposit formation (e.g. Micklethwaite and Cox, 2004; Weatherley and Henley, 2013).

In theory, dilational implosion breccias form when fault slip crossing a dilational jog or step-over suddenly creates a void (Sibson, 1985, 1986; Pavlis et al., 1993). Extreme fluid pressure gradients may exceed the tensile strength of the wall rock, driving spontaneous fracturing (Sibson, 1985, 1986). Sibson (1985, 1986) makes no specific predictions about the orientation of fractures expected in an implosion breccia, beyond suggesting that they may be exceedingly complex. We can predict that Sibson's "implosion breccias" form when fractures open parallel to the fluid pressure gradients, which are ideally radial to the void walls, and stimulate spalling in sheets or flake-shaped clasts (e.g. Valenta et al., 1994). The implosion breccia model of Sibson (1985, 1986) does not necessarily distinguish between seismic slip and slow offset on faults, although it has been used as a seismic signature by numerous studies, and is generally accepted by many workers (e.g. Jébrak, 1997; Okamoto et al., 2006; Griffith et al., 2009a). However, a slow-opening void formed by creep might also fail catastrophically when the pressure gradient reaches a certain level if permeability is sufficiently low or the rock is dry.

Implosion breccias are distinct from attrition breccias, which form by fracturing and grinding along principle slip surfaces during progressive frictional sliding (Sibson, 1986). In either case, the resultant fault rocks are particulate and can be compared according to their particle size distribution (e.g. Sammis et al., 1987). Such distributions are only weakly linked to mechanism, and only end-member dynamically pulverized rock has an interpretable rate-dependence (Wilson et al., 2005; Reches and Dewers, 2005; Rockwell et al., 2010). When an implosion breccia first forms the particles are just inter-fracture blocks with minimal displacement and the breccia can be described by either fracture or particle distribution. We hypothesize that implosion breccias should be distinguishable, by their particle size and shape, from breccia formed by attrition and comminution.

Dynamic fractures (e.g. earthquake ruptures) generate secondary fractures in predictable orientations (Di Toro et al., 2005; Griffith et al., 2009b; Rowe et al., 2012). Experiments demonstrate that the geometry of secondary dynamic mode I fractures depends on the style of the primary rupture (Sharon and Fineberg, 1996; Rosakis et al., 2000; Griffith et al., 2009b; Sagy et al., 2001). Mode I fractures in breccias formed at dilational jogs during dynamic rupture on a fault should display some of these geometric characteristics, distinguishing them from slow or progressive-slip breccias.

We focus on the Pofadder Shear Zone, an ancient, deeply exhumed shear zone located in Namibia and South Africa, where there are known occurrences of overprinted pseudotachylyte (Kirkpatrick and Rowe, 2013) (Fig. 1). In respect to kinematics, scale, rock type and depth of exposure the Pofadder Shear Zone is an ancient analog to the modern quartz plastic transition zone of the southern San Andreas fault, an ideal place to study deep brittle deformation processes occurring on strike-slip systems. We use field studies of natural breccias in the Pofadder Shear Zone to describe numeric and qualitative criteria for the identification of breccias formed by dynamic wall rock fractures. We then define the depth conditions under which brecciation occurred, present a new mechanism for the formation of dilational fault breccia and discuss implications for paleo-earthquake and fault rock studies.

2. Identifying dynamic fracture networks

2.1. Dynamic fracturing: fracture geometry and spacing

Fracture propagation is dynamic when inertia is an important factor in the fracturing process, such as during rapid loading or crack propagation (Freund, 1990). An earthquake is the result of dynamic rupture propagation along a fault plane (Ide and Aochi, 2005). It has been observed in experiments that dynamic ruptures propagating above a critical velocity will produce unique networks of closely spaced secondary tensile fractures (e.g. Sharon and Fineberg, 1996; Griffith et al., 2009b). While the growth of quasi-static extension fractures does not preclude clustering (Delaney et al., 1986), it does encourage localization to fewer main fractures by creating stress shadows (e.g. Price, 1966; Pollard and Segall, 1987; Gross, 1993), and limiting failure to the most favorable flaws (Grady and Kipp, 1987).

Because earthquakes are dynamic ruptures they will produce diagnostic fracturing patterns that cannot be explained by static conditions alone. Analog and field studies of the strain rate dependence of fracturing patterns support the formation of clusters

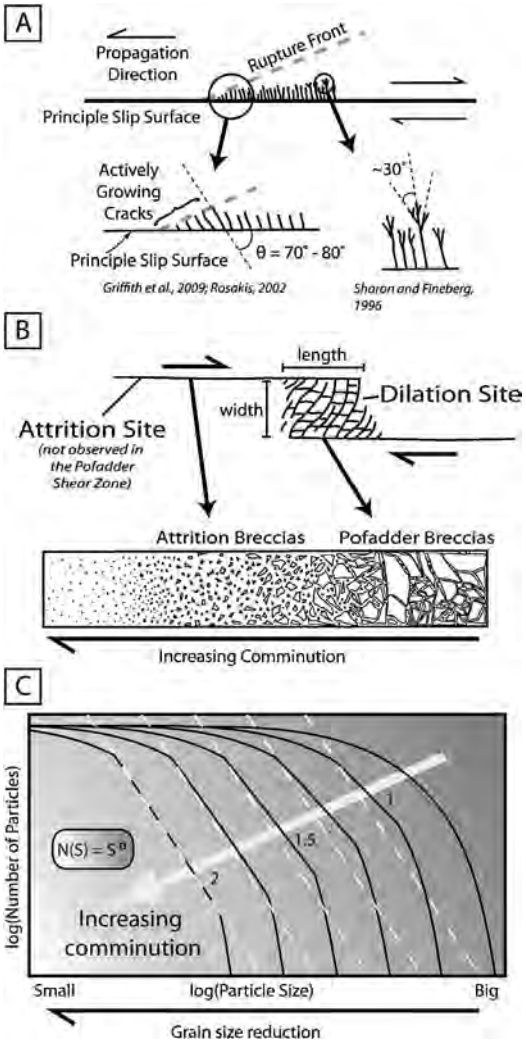

Fig. 2. A) Two styles of dynamic fracture geometries are represented by this schematic drawing, those growing behind the rupture front at high angles (70–80°) from the principle slip surface, and those growing off mode I parent fractures at low angles of ~30°. B) Example of where dilation and attrition breccias occur on a schematic strike slip fault and the associated textures of each. Breccia length and width are also defined. C) Model for the evolution of particle size distributions (PSD) (black lines) with increasing comminution, after Blenkinsop and Fernandes (2000), example D-values are shown. White dashed lines are a reference power-law fit for the PSD at the far left. PSD are meant to roughly correspond to the breccia textures drawn directly above.

of high density fractures and branching fractures at higher strain rates (Sagy et al., 2001, 2006; Rockwell et al., 2010; Riley and Tikoff, 2010) (Fig. 2A). The geometries of secondary dynamic fractures depend on the mode of primary fracture propagation (e.g. Sharon and Fineberg, 1996; Griffith et al., 2009b).

2.1.1. Subsidiary fractures from a dynamic mode II fracture

Dynamic shear rupture experiments demonstrate that tensile microcracks form at high angles of 87–92° (Rosakis et al., 2000) and 70–80° (Griffith et al., 2009b), on one side of the rupture plane within the tensile quadrant (Fig. 2A). The difference in angle between the two studies is ascribed to the rupture velocity and static prestress conditions. Microcracks form an acute angle with the direction of rupture propagation, are closely spaced and can be slightly curved (e.g. Griffith et al., 2009b). These observations match previous laboratory results (Ravi-Chandar and Knauss, 1984) and theoretical predictions (Samudrala et al., 2002; Di Toro et al., 2005). The relation between laboratory-made microcracks and geologic observations of off-fault tensile fractures and pseudotachylyte injection veins was proposed by Rosakis (2002) and supported by Di Toro et al. (2005), Rowe et al. (2012), Griffith et al. (2012), and Ngo et al. (2012).

2.1.2. Subsidiary fractures from a dynamic mode I crack

During primary mode I crack propagation a branching fracture morphology occurs at a critical velocity, above which exists a linear relationship between fracture area and velocity (Fig. 2A) (Sharon and Fineberg, 1996; Sharon et al., 1996). Branching of dynamic tensile fractures has been observed in experiments (Isida and Noguchi, 1992; Sharon and Fineberg, 1996), and predicted numerically (Abraham et al., 1994; Xu and Needleman, 1994) with a characteristic preferred branching angle of ~30°. Sagy et al. (2001) reported a series of clustered fractures with a branching morphology that increase in abundance with proximity to a major strike slip fault. This branching morphology is suggested to form because it is easier for the rock to dissipate energy by forming many branching fractures rather than increasing the propagation velocity on a single fracture (Sharon and Fineberg, 1996). A branching morphology is also observed on a microscale in the densely spaced tabular fracture clusters described by Riley and Tikoff (2010) and in pulverized rocks from deep boreholes (Sagy and Korngreen, 2012).

2.1.3. Fracture spacing

Studies of mode I fracture spacing in layered media find that a "fracture saturation" condition is reached when fracture length (L_f) approaches the fracture spacing (S) (Pollard and Segall, 1987; Wu and Pollard, 1995; Bai and Pollard, 2000a, 2000b). Below a critical value, where $S/L_f \approx 1$, fracture infilling is inhibited. Fracture length can only be as long as the layered medium permits so that at fracture saturation $L_f \approx S \approx$ layer thickness. Extension alone will not form fracture networks with a spacing to length ratio less than half the critical value; for this to occur other mechanisms are required (Bai and Pollard, 2000a). A dilational stepover between two parallel fault segments may be an analogous setting to a stretching layer bounded by two free surfaces, as modeled by Bai and Pollard (2000a, 2000b), therefore, we use their findings as a quasi-static prediction for fracture spacing.

2.1.4. Dynamic fracturing summary

In summary, high angle (70–90°) mode I fractures emanate from the surface of a dynamically slipping fault, forming near the rupture tip with an acute angle to the slip surface in the direction of rupture propagation. They form all along the fault during rupture propagation, leaving a set of parallel fractures decorating the wall rock. These tensile fractures may themselves branch, with subsidiary fractures forming angles of ~30° to the primary tensile fracture (e.g. Fig. 2A). Dynamically growing tensile fractures may form in much closer spacing than is theoretically predicted by quasi-static descriptions of elastic solids, creating a metric by which dynamic fracture arrays may be distinguished in field observations. Where these fracture sets interact between multiple fault surfaces, fracture spacing will correspond to particle size in brecciated rock.

2.2. Particle size distributions

Particle or grain size distributions are used extensively in fault rock studies in order to quantify the self-similarity of fracturing and fragmentation processes (e.g. Sammis et al., 1987; Biegel et al., 1989; Sammis and Biegel, 1989; Marone and Scholz, 1989; Blenkinsop, 1991; Billi et al., 2003; Monzawa and Otsuki, 2003; Billi and Storti, 2004; Heilbronner and Keulen, 2006). Effects of confining pressure, strain, temperature, permeability and deformation mechanisms are manifested in particle size distributions

rendering their analyses an important tool in mechanical fault zone studies (Allegre et al., 1982; Marone and Scholz, 1989; Storti et al., 2003; Hadizadeh and Johnson, 2003; Heilbronner and Keulen, 2006; Keulen et al., 2007; Luther et al., 2013). A particle size distribution is created in log–log space by plotting the cumulative number of particles against their size, the linear portion of the resulting curve is fit with the equation:

$$N(S) = S^{-D} \quad (1)$$

where S is clast size, $N(S)$ is the number of clasts above size S, and D is the slope of the best fit line (D-value). Typically, only the center of the curve is linear, as the particles in larger size classes are underrepresented where size approaches the total size of the studied sample; particles at the lower size classes are underrepresented due to observational detection limits (e.g. Blenkinsop, 1991). However, many particle distribution curves are not log-linear over any grain size range, and cannot be fit with a power law (e.g. Blenkinsop and Fernandes, 2000).

D-values between 1–3 are commonly measured in three-dimensional analyses, corresponding to values of 0–2 when D-value is estimated from two-dimensional observations (Mandelbrot, 1982; Turcotte, 1986; Glazner and Mills, 2012). D-values measured in this study are two-dimensional, measured on outcrop photographs and thin sections. In order to draw comparisons we converted the 3D D-values of other studies to 2D D-values ($D_{3d} = D_{2d} + 1$) (Mandelbrot, 1982).

D-values describe the relative abundance of smaller versus larger clasts, so that increasing the relative abundance of smaller size particles creates a steeper slope and a higher D-value. Because cataclasis reduces particle size and increases the proportion of fine particles, it follows that breccias should have lower D-values than cataclasites or gouge (Fig. 2B, C). Typical 2D D-values for fault breccias range from ~1–1.8 (Storti et al., 2003; Billi and Storti, 2004; Billi, 2005), measured in carbonate fault rocks. Clark et al. (2006) report D-values from fluid induced breccias of 1.17–1.34. Mean D-values of cracked granitoid rock calculated from Table 4 of Keulen et al. (2007) are 1.21 ± 0.11. Cataclasite and gouge 2D D-values are typically higher, clustering around 1.6–1.7 (Sammis et al., 1987; Biegel et al., 1989; Marone and Scholz, 1989), but reaching values as high as 2.5 (see Table 1 of Keulen et al., 2007, for a review). Despite clustering of D-values near 1.6 (e.g. Sammis et al., 1987) many studies find a progressive increase in D-value with increasing cataclasite maturity (Blenkinsop, 1991; Hattori and Yamamoto, 1999; Billi and Storti, 2004; Storti et al., 2007). There is general consensus that D-value increases with increased fragmentation, which is correlated to advancing cataclasis during progressive fault slip. Exceptions to this trend have been suggested by studies linking dynamic pulverization to gouge formation and non-fractal particle size distributions (Wilson et al., 2005; Reches and Dewers, 2005). We expect dynamically formed breccias to have either low D-values or non-fractal distributions (Fig. 2B, C), due to the many similar sized clasts controlled by the characteristic fracture spacing.

3. The Pofadder Shear Zone

The Pofadder Shear Zone is a NW–SE striking, transcurrent, dextral shear zone located in southern Namibia and northwestern South Africa (Fig. 1). This continental-scale structure extends ~500 km, from Lüderitz, Namibia, into South Africa (Joubert, 1974; Toogood, 1976; Coward, 1980; MacClaren, 1988). In the southeast, total right-lateral displacement is ~30 km, based on offset markers and drag folds. Synkinematically emplaced pegmatites within the Pofadder have measured U–Pb monazite ages of 1005 ± 5 Ma and 958 ± 5 Ma (Lambert, 2013), suggesting a minimum duration of activity of 37–57 Ma. Temperatures of deformation are estimated by the presence of synkinematic upper greenschist facies to lower amphibolite facies mineral assemblages equivalent with the lower seismogenic zone to plastic transition zone.

We studied the Pofadder Shear Zone north of the town of Pofadder, South Africa and south of Warmbad, Namibia across three transects perpendicular to the mylonitic fault core (Fig. 1). The transects (Coboop, Kabas, and Pofadder East) are separated along strike by 25 and 6.5 km (Fig. 1).

3.1. Breccia descriptions and field maps

The Pofadder Shear Zone core in the region of Fig. 1 consists of several sharply-bounded, 3–30 m wide high strain zones, comprising planar foliated mylonite and ultramylonite. These high strain zones contain foliation-parallel brittle faults with small right-lateral dilational step-overs of brecciated mylonite (Fig. 3). Lithologies predominantly include meta-granite, with lesser amphibolite, meta-pelite, pegmatite and quartz veins. All breccias in this study occur in similar lithology: granitic mylonites composed of quartz, potassium feldspar and minor plagioclase and muscovite. The grain size in the mylonites is ~10–100 μm.

Breccias occur in intrafolial tabular bodies (Fig. 3A) or with right-stepping rhombohedral to lenzoidal geometries (Fig. 4). Breccia body lengths, measured parallel to the slip direction (as shown in Fig. 2B), range from millimeters to 10s of meters, limited by area of exposure. Widths, measured perpendicular to the slip direction, reach up to 1.5 m but are typically several centimeters to 10 s of centimeters. Typical breccia body aspect ratios are highly elongate in the slip direction (length/width ~10–100), although some have aspect ratios less than 10. These geometries are the result of breccia-forming fracture networks that occur along the length of individual slip surfaces as well as in dilational step-overs (Figs. 3, 4, 5).

Breccias exhibit an exploded jigsaw texture (*sensu* Sibson, 1986) with no internal alignment. Clasts consist entirely of the lithology in which the breccia is hosted, and are commonly square to rectangular in shape (Figs. 3, 5A). No mixing of breccia clasts from distinct and adjacent rock types is observed, indicating that no along-fault clast transport occurred. Breccias are clast-supported, with rare quartz, chlorite and/or epidote cements. No crack-seal textures are observed.

A transition from fractured rock or crackle breccia to a slightly more chaotic, crackle–mosaic, breccia is commonly observed (Fig. 3A). Dense networks or clusters of long, slightly undulatory fractures branch out from brittle slip surfaces which utilize the mylonitic foliation (Figs. 3B–D, 5). These opening mode fractures form at a high angle to the foliation; the apparent angle between the slip surfaces and fractures in Figs. 3B, C and D are $57 \pm 17°$, $90 \pm 14°$ and $50 \pm 23°$, respectively. Fracture surfaces within the breccia bodies do not contain brittle slickenlines or wear products, and breccias are not overprinted by cataclasite or gouge. Fracture spacing, measured in transects parallel to the slip plane, at locations B, C and D of Fig. 3 are 2.4, 2.0 and 2.0 (fractures/cm), respectively. This corresponds to S/L_f (fracture spacing/fracture length) values of $\leq$0.07, 0.17, 0.05.

3.2. Map relationships

The Kabas location (Fig. 4) displays the typical strong foliation of the host mylonites and ultramylonites, with fault-parallel and cross-cutting breccia lenses. The mylonitic foliation is slightly undulatory with a mean orientation of 312/81NE. Brittle ridge-in-groove slickenlines and quartz-plastic stretching lineations measured on C surfaces (ductile striations *sensu* Lin et al., 2007) have

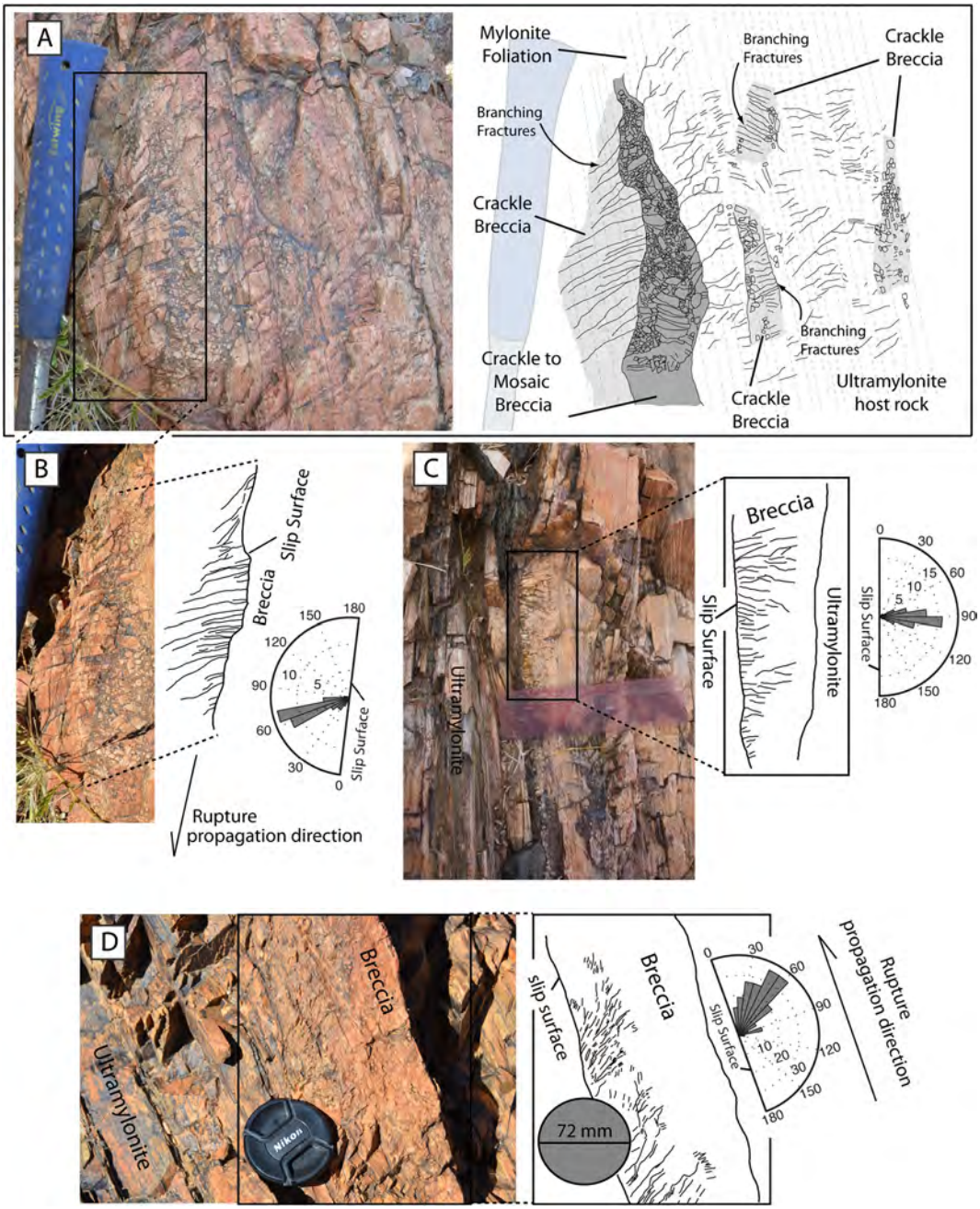

Fig. 3. A) Field photo and interpretive sketch of crackle–mosaic breccia and dynamic fracture networks in host ultramylonites, zones with different degrees of brecciation are highlighted in shades of gray. All slip is dextral even though rupture directions vary. B), C), D) Examples of dynamic fracture networks, with fractures forming high angles to the principle slip surface and the mylonitic foliation. These angles can indicate rupture propagation directions following Griffith et al. (2009b).

the same range of orientations (Fig. 4), signaling that the slip direction did not change during transitions from plastic to brittle deformation. The mean plunge of lineations is 50° NW (Fig. 4).

At the Kabas location, breccias cross-cut the foliation at ~30° and vary in length from 0.08 to 1.17 m, measured parallel to the fault slip direction (see Fig. 2B). Slip-parallel breccia bodies range from sub-cm to 7 cm width with a lot of along-strike variability and most often occur within ultramylonites. These breccias are bounded by two parallel slip surfaces, represented by thick dashed lines in Fig. 4, there is no wear material on fault-parallel slip surfaces, and breccia clasts show no evidence of attrition or grinding.

The largest breccia pod at the Kabas location contains an undulatory fracture network at a high angle to both the fault and the edge of the breccia body (Fig. 5). Measured on outcrop surfaces, the apparent angle between the fault and the tensile fractures is $53 \pm 14°$; this is an apparent angle as it was not measured normal to the intersection of the two fracture types. Opening mode fractures within the breccia body have a 33° difference in strike from surrounding outcrop joints (Fig. 5D), suggesting they formed under different stress conditions. The average joint spacing away from the breccia bodies was measured at two locations (1 and 2 in Fig. 4), at 0.31 and 0.19 fractures/cm. Fractures within the breccia body (number 3 in Fig. 4) have a fracture density of 1.1 fractures/cm, and an S/L_f, spacing to length ratio, of 0.01.

Similarly detailed maps from the Pofadder East transect reveal consistent breccia dimensions and geometries. Details are presented in the supplement.

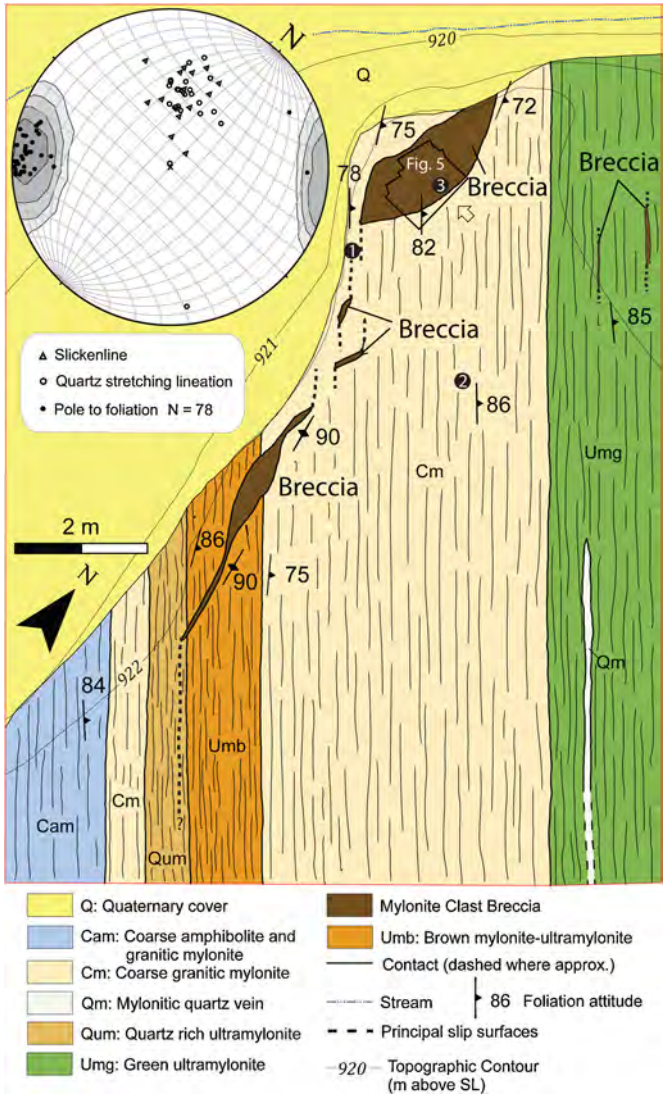

Fig. 4. Field map of the Kabas location showing well-foliated mylonites of the Pofadder Shear Zone core and cross-cutting to foliation subparallel breccia body geometries. Lower hemisphere stereonet demonstrates consistent foliation, and overlap of quartz plastic stretching lineations and brittle ridge-in-groove slickenlines. Map units are divided based on intensity of foliation and grain size as well as lithology, with all breccias mapped as a single unit regardless of rock type. Mylonitic foliation is diagrammatically shown with sketched sub-parallel lines.

3.3. Conditions and depth of faulting

Microstructural studies of the Pofadder breccias reveal two lines of evidence for static quartz-plastic recovery, post-brittle deformation: 1) a long axis breccia clast shape fabric in some breccias and, 2) a bulging grain boundary morphology in quartz cements (Fig. 6A–F). Furthermore, a relative age relationship is suggested by breccia truncation, as shown in Fig. 6A, indicating that multiple generations of brecciation occurred, separated by periods of crystal plastic recovery.

Strong long axis breccia clast shape fabrics, such as those presented in Fig. 6B, have been previously linked to a ductile overprint (Sibson, 1977). In places, clast boundaries are difficult to distinguish from recrystallized cement (Fig. 6C) and some of the larger clasts appear to comprise many annealed small clasts, especially within breccia layer b1. The age relationship apparent in Fig. 6A (b1 > b2) means that b1 would have experienced a greater degree of plastic overprinting. It appears that during plastic recrystallization clasts begin to anneal together and increase in length adopting a long axis that is sub-parallel to the mylonitic foliation. The geometry of the annealed clasts suggests a strong component of foliation-normal (also fault-normal) compaction. The truncation relationship between breccias b1 and b2 suggests that while brecciation follows the host rock anisotropy the original slip surface has been restrengthened. In this case, restrengthening can be attributed to plastic recovery, because both breccias have been overprinted.

Tortuous grain boundaries in the quartz cement are consistent with post-cementation dynamic recrystalization (Passchier and Trouw, 2005) (Fig. 6D–F). Recrystallized cement comprises ~10–50 μm quartz grains with a short wavelength boundary migration texture diagnostic of bulging recrystallization (e.g. Stipp et al., 2002). Bulging recrystallization, in quartz, occurs between ~280–~400 °C (Stipp et al., 2002).

It is difficult to recognize plastically overprinted breccia in the field, and those we do observe display dominantly a foliation-normal flattening. It is likely that a small degree of plastic, simple shear strain renders breccias unrecognizable. However, these observations clearly demonstrate that brittle fracturing and breccia formation took place at temperatures suitable for plastic recovery of quartz and possibly potassium feldspar, consistent with temperature estimates from the quartz microstructure. In the granitic crust, this temperature range (~300–400 °C) is consistent with the lower seismogenic to plastic transition zone (Sibson, 1984), where fracturing is expected at high strain rates while plastic recovery can follow at low strain rates (Sibson, 1983; Scholz, 1988). Given an active margin geothermal gradient of ~25–30 °C/km (Lachenbruch and Sass, 1977), this transition would occur at depths of ~10–16 km.

4. Particle size distributions: calculating fractal dimensions

Above we proposed to use particle size distributions in order to develop a quantitative method for distinguishing dynamic breccias. We compare our predictions to observed grain size distributions for 8 breccia samples from the Coboop and Kabas transects. Automated clast detection was not possible because breccia clasts contain multiple phases of different colors, therefore manual outlining of breccia clasts was required. Breccia clasts were outlined on scaled photographs with the use of a drawing track pad (Figs. 5B, 7B). The resultant black and white images were imported into Matlab and breccia clast size was measured with use of the "Gray Scale Image Analysis" program, which defines clasts based on a gray scale intensity value (Bjørk, 2006a, 2006b; Bjørk et al., 2009).

Equivalent diameter breccia clast size distributions were plotted and a best fit line for the log-linear portion of the distributions was fit using the "Snap, Crackle, Pop" (SCP) script (digital supplement). The SCP script allows the log-linear portion of the curve to be selected by hand at distinct changes in slope and calculates a best fit power-law by linear regression. Hand picking the power-law limits is appropriate when the log-linear portion occurs at intermediate size values and an exponential relation does not adequately describe the distribution (Blenkinsop, 1991). SCP allows the user to optimize line picking to maximize best fit parameters.

We measured D-values of samples spanning the full range of observed deformation textures, from crackle textures to breccias with a more chaotic appearance. Sample textures were qualitatively defined and selected by the degree of clast interlocking and rotation. We then compared the D-values with qualitative textural descriptions of the breccias made in the field and in thin section. D-value results range from 0.89–1.90 with a mean of 1.47 ± 0.37 (Fig. 7).

Results show that breccia D-values are low in comparison to comminution products, and that as crackle breccia textures

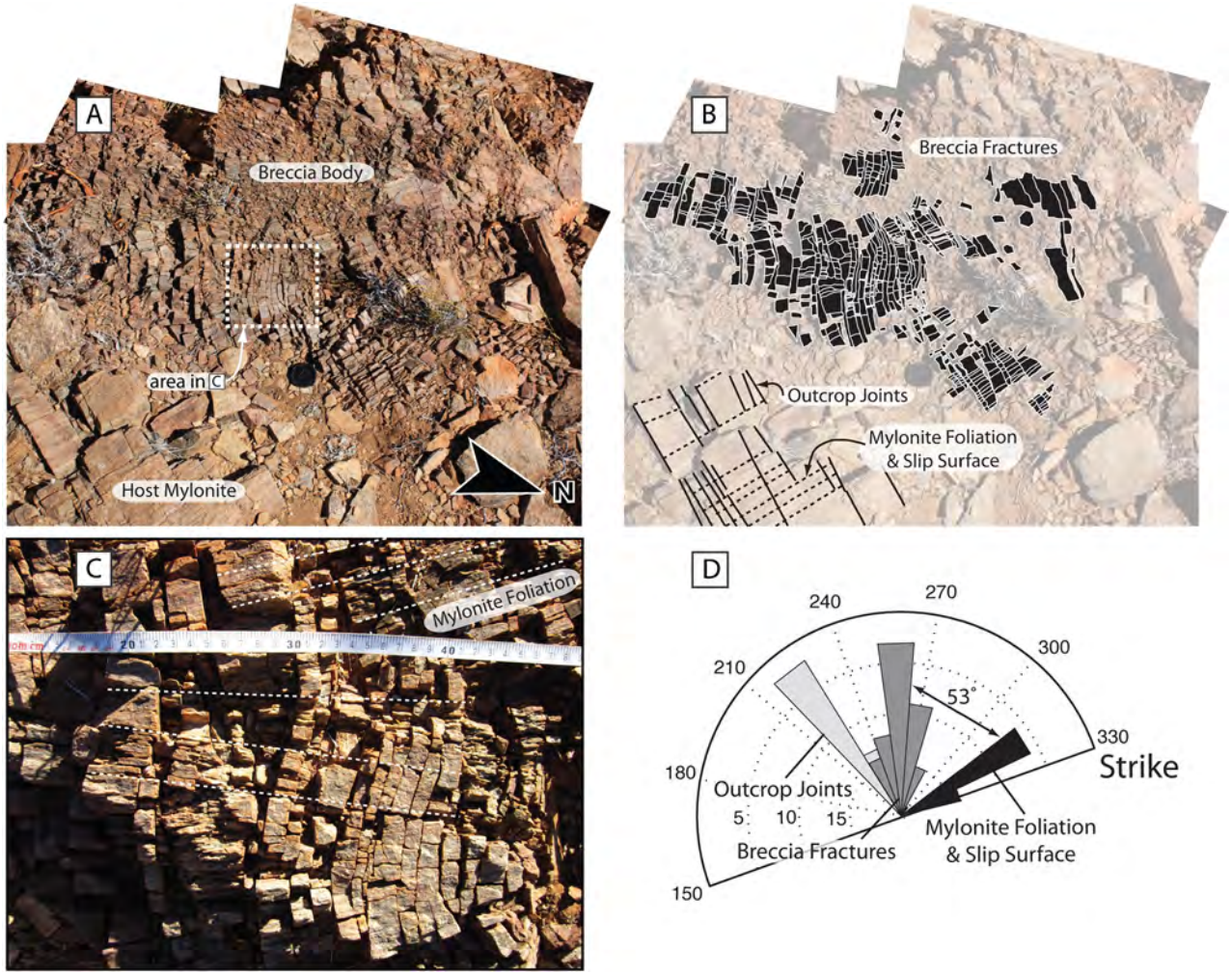

Fig. 5. A) Field photo of largest breccia body at the Kabas location showing the host mylonite in the bottom left corner. The photo was taken at the spot marked on Fig. 4 and the lens cap is included for scale (58 mm). B) Breccia clasts are outlined in this photograph, these black and white images were used for clast counts and size distributions. Dashed and solid lines in the host mylonite highlight the mylonitic foliation and outcrop joints. C) Dense, sub-parallel, undulatory fracture network, with breccia clasts formed by the intersection of the mylonitic foliation and the fractures. The mylonitic foliation (dashed in white) has been rotated as clasts begin to form. This is a zoom into the white dashed box in A. D) Dynamic fractures at this outcrop form a high apparent angle ($53 \pm 14°$) with the mylonitic foliation and slip surface, they have a distinct orientation from outcrop joints.

become more chaotic the D-value increases. This transition is exemplified in samples PS194a,b (Fig. 7B) where an abrupt boundary between two distinct breccia textures occurs. However, there was one major exception. Crackle breccia sample PS204 has a D-value of 1.85, while other crackle breccias have low D-values (PS194b = 0.89) or are not log-linear distributions (PSKB, PSON). All four of these samples are at the beginning stages of brittle deformation and display primary dynamic fracture networks (Fig. 7 and Fig. 5). The reasons for the outlying PS204 D-value are discussed below in Section 6.2.

Two distinct D-values occur in two of the samples measured: PS126 and PS195, both samples are some of the most chaotic that we measured. Both sets of D-values were included in the mean presented above. The distinct changes in slope defining the different D-values occur at 0.81 and 0.85 mm, respectively, and are marked with solid black arrows in Fig. 7. Lastly, there are steps in the particle size distributions at larger clast sizes, highlighted by the hollow arrows in Fig. 7.

5. Discussion of geologic relationships

Pofadder breccia textures and geologic relationships, described above, contain the key to differentiating between fast and slow breccia formation. The dilational fractures emanating from the fault surfaces (Fig. 3A, B) are equated to those produced in Homalite-100 experiments (Rosakis, 2002; Griffith et al., 2009b), whose spacing and angle to the fault are indicative of the dynamic rupture propagation direction on the fault. These fractures themselves are observed to branch at their tips (Fig. 3C, D), similar to dynamic propagation of primary tensile cracks (e.g. Sharon and Fineberg, 1996).

The dilational breccias we have described formed by the intersection of off-fault dynamic mode I fractures and the mylonitic foliation in the wall rock. This is distinct from previous descriptions of dilational implosion breccias formed by high fluid pressure gradients (Sibson, 1985, 1986; Valenta et al., 1994; Jébrak, 1997; Clark et al., 2006). The mylonitic foliation plays an important role in breccia formation, by serving as the slip surface and controlling breccia body and clast shapes. This is evident by the common tabular intrafolial breccia morphologies and the rectangular to square-shaped clasts (Fig. 5). The foliation is a plane of preexisting weakness, which preferentially breaks during brittle deformation, connecting dynamic fractures and forming breccia clasts. Additionally, mylonitic surfaces are stronger than pure frictional interfaces, leading to larger off-fault normal stress perturbation associated with rupture (e.g. Ngo et al., 2012). The mylonitic foliation

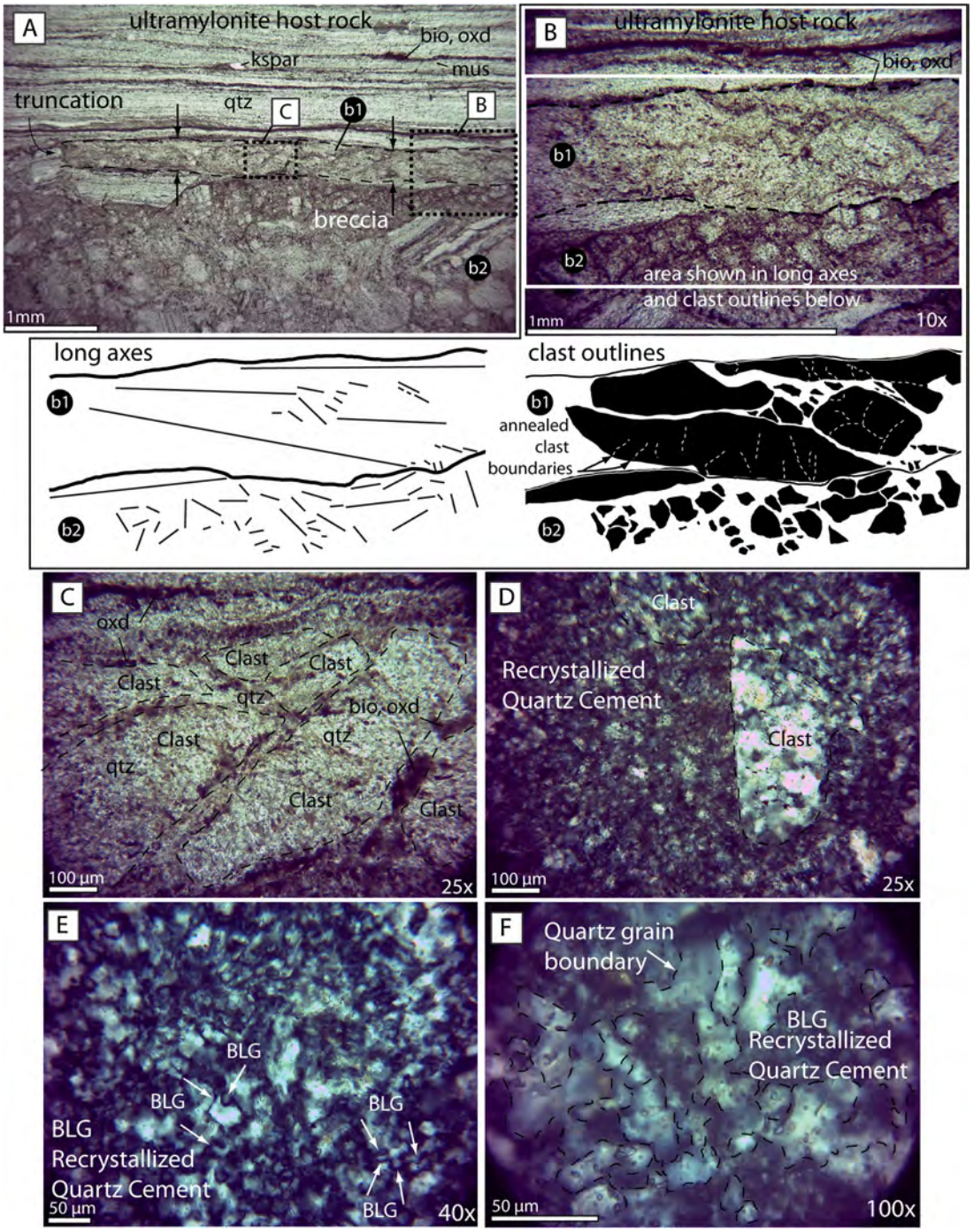

Fig. 6. A) Photomicrographs of sample PS182 showing abrupt transition from ultramylonite to breccia. Breccia layers occur in a foliation subparallel geometry. Dashed boxes mark locations of photographs in B and C. b1 – breccia one, b2 – breccia 2, qtz – quartz, bio – biotite, oxd – oxide, mus – muscovite, kspar – alkali feldspar. B) Breccia clasts from layers b1 and b2 are distinct in their size and orientation, small annealed clasts are visible in larger amalgamated clasts. Sketches show long axes orientations and clast shapes in black, white dashed lines are annealed clast boundaries. C) Clasts in breccia layer b1 are sometimes hard to discern from the matrix. Clast outlines are dashed in black. D) A comparison of recrystallization texture in cement and clasts, cement is composed of fine grained dynamically recrystallized quartz. E) Example of bulging recrystallization in the cement, arrows point out bulging grain boundaries. F) Another example of bulging recrystallization in the quartz cement. Dashed black lines show quartz grain boundaries.

occurs on a $\leq$1 mm scale, so the favorable surfaces for foliation-parallel fracture are much more closely spaced than the foliation-perpendicular dynamic fractures (Figs. 4, 5). However, the mean clast aspect ratio is 2.6, with long axes that tend to occur perpendicular to the slip surface (see Fig. 5C, and samples PSON and PS194b in Fig. 7B). This suggests that dynamic fractures control the initial clast shape as well as the foliation-parallel fracture scale.

Implosion breccia formation was originally proposed to be driven by a fluid pressure differential created by dilational jog opening during slip (Sibson, 1985, 1986). The same pressure condition has been shown to cause catastrophic precipitation of amorphous silica or quartz cements in faults at similar depths and tectonic settings (e.g. Weatherley and Henley, 2013). Therefore, the lack of a hydrothermal cement in the Pofadder breccias may imply that fluid pressure drop is not an appropriate explanation for

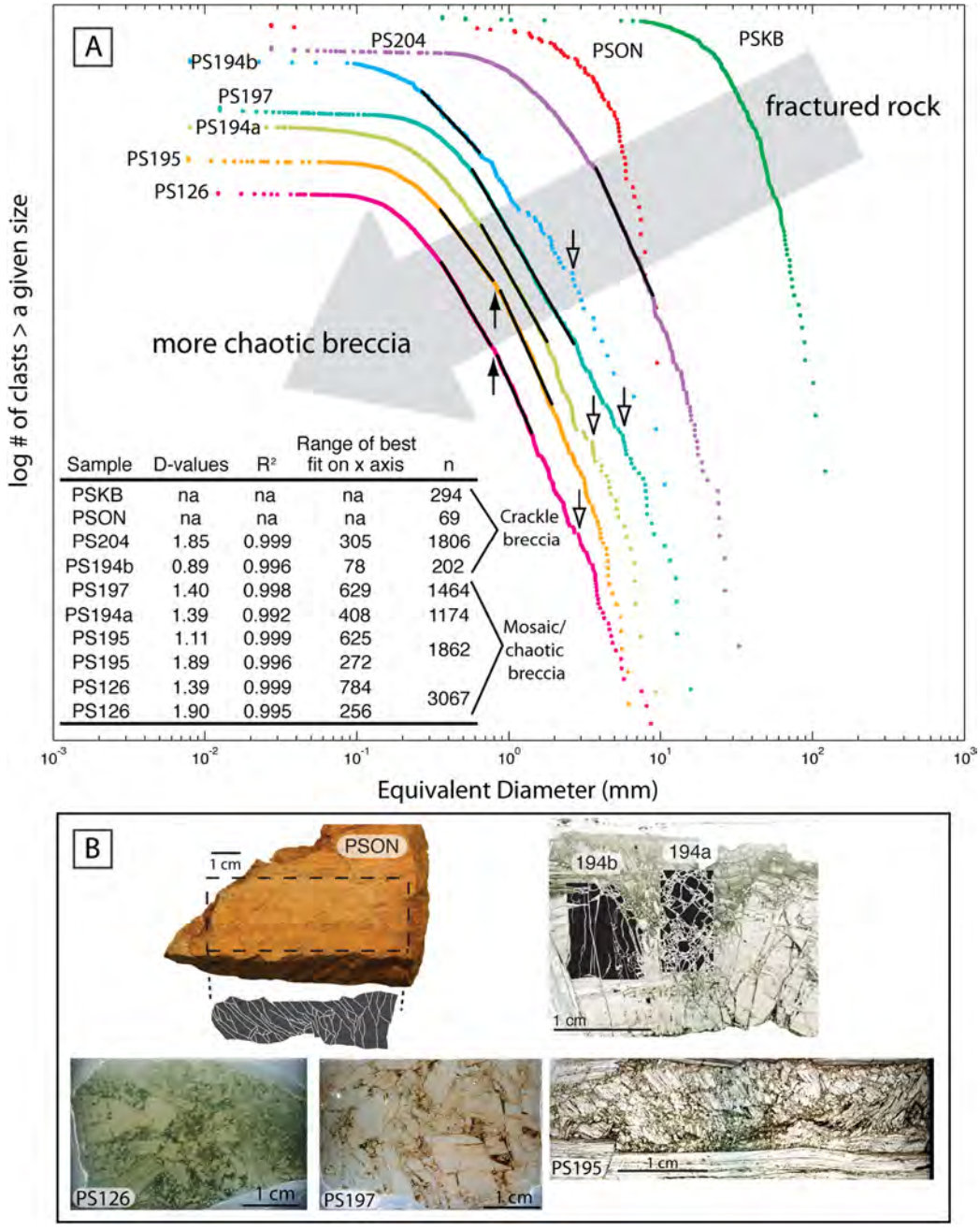

Fig. 7. A) Particle size distributions of all samples analyzed during this study with solid black best fit lines. *D*-values are presented in the table, the repeated samples have two power-law fits. Gray arrow shows progression from fractured rock to a more chaotic breccia. Small black arrows highlight distinct changes in slope in the distributions and the hollow arrows highlight some examples of steps or shelves in the distribution. The clast distributions have been vertically offset for ease of comparison, as a result the *y*-axis has no scale. B) Images of analyzed samples including black and white clast outlines of PSON, PS194a and PS194b. All images are thin section photographs with the exception of hand sample PSON. Samples PS204 and PSKB are shown in Figs. 3C and 5A–C.

brecciation in this case. In addition, the breccia clast shape and fracture morphology are consistent with the predicted dynamic fracture patterns, not with concentric wall-failure around a void. Most Pofadder breccias are clast-supported, and healing between brecciation events is dominated by plastic processes rather than cementation. We must consider the possibility that because breccias create fluid flow pathways, chlorite, epidote, and rare quartz cements may have been deposited by later groundwater flow, especially since the majority of breccias are not cemented. We contend that the Pofadder breccias described here formed through the development of dynamic fracture networks without requiring transient high fluid pressure gradients, although these effects may have existed simultaneously.

In summary, the geologic relationships presented above suggest a new mechanism for coseismic dilational breccia formation. The unique clast size relationships and fracture geometries can be incorporated as part of a new paleoseismic tool. Our observations of fracture networks in Pofadder breccias match remarkably well with previous experimental studies (e.g. Sharon and Fineberg, 1996; Griffith et al., 2009b), and lack attributes expected in a fluid pressure gradient-driven implosion breccia (e.g. Sibson, 1986). Because we observe secondary tensile fractures that branch off both primary mode I and mode II fractures, we recognize a possible link between these two experimental cases. Because our observations are made on outcrops occurring at a variety of angles from the slip vector, we are confident that we have documented the full

array of fracture geometries. Our data suggest that Pofadder breccias formed in single events without continued grinding or clast transport and the mylonitic foliation served as a principle slip surface during brittle slip. Lastly, quartz plastic static healing of some breccias places a depth constraint on breccia formation, below the quartz plastic transition.

6. Discussion: dilational breccias as signals of deep fault seismicity

In this paper we recognize a new mechanism for dynamic (coseismic) breccia formation near the quartz-plastic transition. This leads us to define this new mechanism, and ultimately establish the foundation for a new paleoseismic indicator. In this section we focus on the development of a paleoseismic tool, discussing the primary geologic attributes that characterize an earthquake breccia as well as the validity of using D-values to assist in their quantification. We present a new time sequence model for earthquake breccia formation, as suggested by the geologic relationships presented above (Section 5). Finally, we estimate earthquake magnitudes and rupture distances, and in combination with geologic evidence, infer the depth of earthquake nucleation.

6.1. Fracture morphology and density

Unique fracture morphology and density are perhaps the most important attributes for recognizing dynamically formed breccia. Above, we argued that the secondary mode I fractures emanating from brittle fault surfaces were analogous to dynamic wall fractures formed during dynamic slip pulse propagation in Homalite-100. Not all our observations of fracture angle match perfectly with analog experiments; the variation in fracture angle is as much as 20° (Fig. 3) from the observations of Griffith et al. (2009b) (Figs. 2A and 3). The variations likely arise from differences between the experimental setup and what is observed in nature. These include: 1) a non-planar natural fracture surface and, 2) a homogeneous experimental medium. The mechanical interaction with surrounding weaknesses such as the mylonitic foliation or other fracture surfaces may significantly alter predictions made in homogeneous solids (Rosakis et al., 2000). Additionally, this difference in angle might be related to a variation in the near tip stress field caused by the frictional behavior of the fault rocks or shear strength of the rupture surface. As the overall geometry of fracture systems is maintained between breccias and readily distinguishable from the predictions of quasi-static fracture distributions, we interpret the variance in mean angle from the Homalite-100 experiments to be caused by differences in material properties.

It is suggested by the sub-parallel curvature of adjacent fractures (e.g. Fig. 5C) that fracture propagation is affected by stress perturbations ("shadows") caused by the presence of nearby fractures. This is evidence of the simultaneous growth of breccia-forming fractures contained between two free surfaces. It is important to note that fracture networks are not healed or cemented. This means rock strength was never restored, and precludes a model of fractures formed cumulatively by successive jointing and healing. Bai and Pollard (2000a) state that extension alone cannot account for fracture spacing less than half the critical value of $S/L_f = 1$, and another mechanism must be invoked to account for such low values. Dynamic Pofadder breccias have S/L_f values as low as 2 orders of magnitude below the critical value. We recognize that quasi-static conditions can form fracture clusters (e.g. Delaney et al., 1986), however with continued deformation they will tend to localize. In contrast, Pofadder breccias formed almost instantaneously and are evenly distributed throughout the wall rock. This leads us to a model of strain rate dependent crack spacing. We expect that a rapid increase in tensile stress will be more effectively dissipated by growing many fractures, therefore the rate of tensile stress increase may be inversely proportional to crack spacing.

Fig. 8 is a schematic representation of the time evolution of a breccia body based on observational constraints. At time one (t1) the rupture surface forms on a pre-existing weak plane parallel to the mylonitic foliation. The rupture front propagates from right to left forming a network of dynamic tensile cracks. These fracture networks are not restricted to dilational jogs. At time two (t2) the rupture passes through a dilational jog, either stepping over or rupturing two fault surfaces simultaneously. Fractures propagate into the jog, intersecting the mylonitic foliation and creating clasts. Clast rotation is at a minimum and clasts have similar sizes. At time three (t3) the earthquake rupture has passed and the total slip increment has occurred. Breccia clasts rotate to their maximum extent, as they do so they continue to break, creating a larger proportion of smaller clasts and a self-similar size distribution. At t3 the breccia has reached the final state of disorganization, no continued slip or grinding occurs, and the slip surface has time to restrengthen by crystal plastic mechanisms.

6.2. Breccia particle size distributions

We quantify Pofadder breccia D-values in order to test a potential set of attributes unique to dynamic breccia textures and develop a new paleoseismic tool. We find that particle size distributions (and D-values) are important, but must be used in concert with fracture network geometries and geologic relationships. Crackle breccias, in which the primary dynamic fracture network can be identified, typically do not display self-similarity because clasts have a very uniform size (PSKB, PSON, PS194b, PS204) (Fig. 7). Such distributions may be described with an exponential or linear relationship, similar to dynamically pulverized material with little to no shear strain (Rockwell et al., 2010) (far right curve in Fig. 2C). A self-similar geometry develops as breccia clasts begin to rotate and fracture, destroying the initial dynamic fracture network. However, sample PS204 which displays a dynamic fracture network, has a relatively high D-value (Figs. 3C, 7), reinforcing that particle size distributions alone may be insufficient to distinguish dynamic from continued comminution breccias. This is further supported by the fact that the D-values from this study overlap D-values from studies of cataclasites and gouge. We attribute high D-value from PS204 to the fact that during dilatancy there is an increased ability for small particles to rotate and break (Keulen et al., 2007), resulting in a rapid decrease in particle size for particles smaller than the crack aperture. The implication is that D-values will rapidly increase with relatively small amounts of slip. In fact, our mean D-value is similar to other studies of cracked grains (Keulen et al., 2007), and other dynamic fracture settings (Buhl et al., 2013).

Two of the samples investigated display particle size distributions with two distinct segments of different slopes. Samples PS126 and PS195, which are some of the most chaotic samples we studied, display an abrupt change in slope marking two linear portions of the curve. This change in slope is marked by the black arrows in Fig. 7A, and is located at approximately the same clast size (~0.8 mm). Low D-values are observed at smaller clast sizes and greater D values at larger clast sizes, very similar to what Keulen et al. (2007) report. This suggests that as a breccia forms it is relatively easy for clasts above a given size threshold to become smaller, but once that threshold is reached (~0.8 mm for our breccias) it becomes harder for breccia clasts to reduce in size. Unlike Keulen et al. (2007), however, we cannot attribute this to a grinding limit because clasts are large and have not experienced continued grinding and attrition. This threshold, in our rocks, is likely related to a strength increase caused at the preferred size

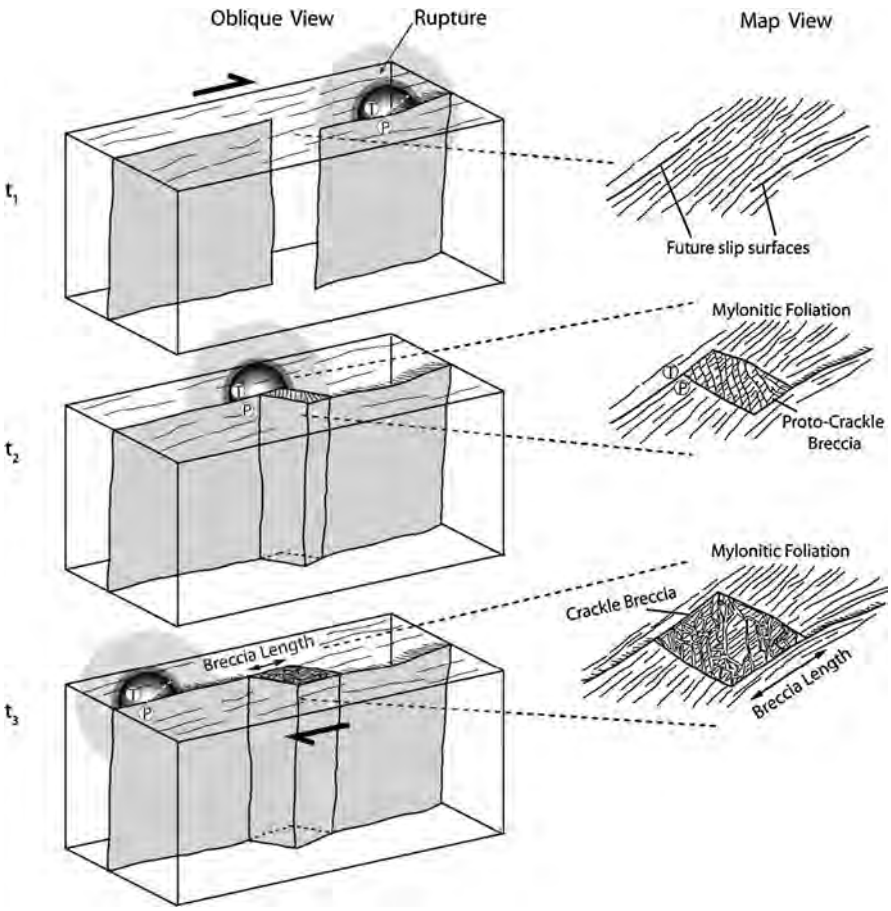

Fig. 8. Interpretive 3 dimensional breccia development model between time 1 and 3 (t1–t3), with schematic map view breccia bodies drawn on the right. Gray shading represents fault plane and breccia body volume, fractures are only shown on the surface for clarity, but would continue to depth. The rupture tension and compression fields are represented by T and P symbols. t1 – rupture propagates along foliar surface in mylonite approaching the site where it will step over. t2 – rupture passes through step-over, dynamic fractures growing behind the rupture front explode the wall rock. Rupture either steps over or two parallel surfaces slip simultaneously over a short distance. t3 – the rupture has passed and the final state of brecciation has been reached.

of porphyroclasts and mylonite laminae widths of the host rock, which are <1 mm (Fig. 6).

Steps in the particle size distributions are a manifestation of many similar sized clasts formed by the intersection of dynamic fracture spacing and the mylonitic foliation (Fig. 7). Dynamic fracture spacing appears to vary with breccia body size, as demonstrated by the large spacing in PSKB, which has a mean clast size one order of magnitude larger than all the other samples (Fig. 5). Although this supports a model for breccia width control on dynamic fracture spacing, there may be other variables at play, including coseismic friction evolution, rupture speed and direction, magnitude or slip distance. These steps are the subject of ongoing investigation.

6.3. Estimating earthquake magnitudes

We estimate earthquake magnitudes for the simplest case where displacement across the breccia bodies is equivalent to displacement in one earthquake, and events followed typical earthquake scaling. The displacement is approximated by the amount of opening parallel to the slip direction that formed each breccia body (Fig. 2B) (Griffith et al., 2009a). For a rough 2D approximation, we use the area (in %) of each breccia body occupied by clasts to estimate the void area created during slip (where 100% − % clasts = void area). Since each breccia is bounded by two faults whose separation remained constant (Figs. 4, 8), we assumed the slip parallel to the fault was proportional to area. Therefore, the slip distance ($\bar{d}$) becomes:

$$\bar{d} = l \times (100\% - a) \tag{2}$$

where a is the percentage of each breccia body occupied by clasts in 2D, and l is the breccia body length parallel to the slip direction in the plane of the fault (Fig. 2B). The mean value of a calculated from 8 breccias is approximately 85%, corresponding to a void space of 15%. Although this is a rough estimate, will likely underestimate 3D porosity and does not account for complexities observed in the field, it provides a basis for comparing dilation between breccias. The consistency of our observations across different scales supports use of a single dilation value for different magnitudes. Measured values for l and calculated $\bar{d}$ for 5 dilational breccias are given in Table 1.

We assume an equidimensional rupture area with length L, and typical static stress drops ($\Delta\sigma$) of 1 and 10 MPa (Ide and Beroza, 2001). Using the equations for static stress drop and seismic moment on a strike slip fault (Kanamori, 1977; Lay and Wallace, 1995), we solve for seismic moment:

$$L = \frac{2\mu\bar{d}}{\pi\Delta\sigma} \tag{3}$$

$$M_o = \frac{\pi}{2}\Delta\sigma L^3 \tag{4}$$

where the shear modulus (μ) is 30 GPa (e.g. Kanamori and Brodsky, 2004). The seismic moment was then used to calculate the moment magnitude using the equation from Kanamori and Brodsky (2004):

Table 1
Estimates of slip distance, rupture length and earthquake magnitude.

Location	Breccia length (l) (m)	Slip distance ($\bar{d}$) (m)	Calculated rupture length (L) (m)	Seismic moment (M_o) (Nm)	Moment magnitude (M_w)
1 MPa static stress drop					
Kabas	1.17	0.18	3347.2	5.90×10^{16}	5.1
Kabas	0.22	0.03	629.4	3.92×10^{14}	3.7
Kabas	0.08	0.01	228.9	1.89×10^{13}	2.8
Kabas	0.71	0.11	2031.2	1.32×10^{16}	4.7
Pofadder East	0.2	0.03	572.2	2.95×10^{14}	3.6
10 MPa static stress drop					
Kabas	1.17	0.18	334.7	5.90×10^{17}	5.8
Kabas	0.22	0.03	62.9	3.92×10^{15}	4.3
Kabas	0.08	0.01	22.9	1.89×10^{14}	3.4
Kabas	0.71	0.11	203.1	1.32×10^{17}	5.3
Pofadder East	0.2	0.03	57.2	2.95×10^{15}	4.2

$$M_w = \frac{\log(M_o)}{1.5} - 6.07 \quad (5)$$

Estimated magnitudes range from M_w 2.8–3.4 for the smallest measured breccias, and up to M_w 5.1–5.8 for the largest (Table 1). Assuming typical scaling, these values correlate to rupture lengths ranging from 0.023–3.3 km (Table 1). We observe brittle surfaces in the Pofadder Shear Zone 10s of meters in length (restricted by outcrop extents) at the three transects (1, 2, and 3, Fig. 1), separated by more than 30 km. Therefore, it is possible that earthquake ruptures of this size occurred on the Pofadder Shear Zone. The validity of estimating the magnitude of such small earthquakes is supported by the self-similarity of events as small as -1 M_L (Abercrombie and Leary, 1993; Abercrombie, 1995).

6.4. Tectonic setting

Earthquakes in the quartz-plastic transitional zone are not uncommon due to the large strain rate fluctuations inherent to this region of the crust (Hobbs et al., 1986). An earthquake nucleating in the lower seismogenic zone can propagate down fault causing a sudden change from quartz plastic flow to brittle failure (e.g. Sibson et al., 1975). Alternatively, earthquakes might nucleate in the transitional zone caused by strain localization at a ductile instability or at strength contrast boundaries (e.g. Sibson, 1977, 1980; Hobbs et al., 1986; White, 2012). Down fault propagation is a possible explanation for ruptures large enough to span the transition zone, but small ruptures must have nucleated within the transitional zone. Although our earthquake magnitude estimation is rough, it is useful when considering the mechanism by which the earthquakes occurred.

If our estimates of $\bar{d}$ represent the average slip over the slip area, then these earthquakes are too small to have propagated down dip, and must have nucleated in the transitional zone. Because we can only estimate one slip distance value from each breccia we have no way to calculate mean slip or variance, which is assumed in the scaling relationships we use. Regardless, our estimates suggest that these are small to moderate earthquakes, some of which probably nucleated within the zone of quartz plasticity, and that re-strengthening by plastic creep after these events may have restored nearly all of the rock strength.

While it is likely that some syndeformational exhumation occurred in the Pofadder Shear Zone, the lack of gouge or cataclasite precludes extended grinding and comminution in the brittle regime. This and the existence of a plastic overprint requires alternative mechanisms for breccia formation other than exhumation into the brittle regime.

7. Conclusion

While we have described dynamic fault breccias from a mid-crustal shear zone, similar breccias likely form through-out the seismogenic crust in a variety of tectonic settings or rock types. Here we summarize some of the universal defining characteristics of dynamically formed, single-slip dilational breccias:

- They comprise densely spaced, sub-parallel, tensile fractures which bifurcate off primary slip surfaces at high angles and are, in some places, undulatory and locally branching at their tips.
- They exhibit an exploded jigsaw texture with minimal clast rotation and displacement, have monomict, locally sourced clasts, and lack wear products on slip surfaces or within the breccia body.
- They are dominantly clast supported.
- They display a relatively low D-value, or are best fit with an exponential function.
- They display an often abrupt transition from crackle to mosaic breccia textures.
- They are not restricted to dilational jogs.

The significance of our work is four fold: 1) We have recognized a new paleoseismic fingerprint based on fracture geometry, geologic relationships and particle size distributions. 2) We have identified a new mechanism for the formation of dilational breccias. Pofadder breccias are distinct from “implosion breccias” (*sensu* Sibson, 1986) because they were not formed by pressure gradient-driven failure of the walls of a void, but rather by the intersection and interaction of dynamic, near-fault, fractures associated with an earthquake rupture. 3) We recognize that D-values alone are insufficient in quantifying dynamically formed breccias. This is due to the many complexities and varying mechanisms operating during breccia formation. Particle size distributions are important and can help classify dynamic dilational breccias, however, they are meaningless without the correct geologic context. 4) Finally, Pofadder breccias formed over a depth range equivalent to the quartz plastic transitional or lower seismogenic zone, and constitute a newly-recognized manifestation of deep seismic slip. Dynamic dilational breccias, at any crustal level, form coseismically and can be applied in future fault zone studies as signals of seismic slip.

Acknowledgements

We acknowledge Dr. Yajing Liu and Dr. Rebecca Harrington for helpful discussions about earthquake scaling and the basics of Matlab, Dr. Kisters for his support, the contributions of field assistants Timothy Sherry and Tanya Dreyer, and helpful feedback from Nils “Pug-On-Wheels” Backeberg. This paper was greatly improved by the helpful reviews of Dr. Ashley Griffith and an anonymous reviewer. We thank the Carstens family at the Lekkerbly Hostel in Pofadder, South Africa, for the hospitality. This work was supported by a 2011 GSA student research grant and the Robert P. Wares faculty scholarship.

Appendix A. Supplementary material

Supplementary material related to this article can be found online at http://dx.doi.org/10.1016/j.epsl.2014.07.002.

References

Abercrombie, R.E., 1995. Earthquake source scaling relationships from −1 to 5 M_L using seismograms recorded at 2.5-km depth. J. Geophys. Res., Solid Earth (1978–2012) 100 (B12), 24015–24036.

Abercrombie, R., Leary, P., 1993. Source parameters of small earthquakes recorded at 2.5 km depth, Cajon Pass, southern California: implications for earthquake scaling. Geophys. Res. Lett. 20 (14), 1511–1514.

Abraham, F.F., Brodbeck, D., Rafey, R., Rudge, W., 1994. Instability dynamics of fracture: a computer simulation investigation. Phys. Rev. Lett. 73 (2), 272.

Allegre, C., Le Mouel, J., Provost, A., 1982. Scaling rules in rock fracture and possible implications for earthquake prediction. Nature 297, 47–49.

Bai, T., Pollard, D.D., 2000a. Closely spaced fractures in layered rocks: initiation mechanism and propagation kinematics. J. Struct. Geol. 22 (10), 1409–1425.

Bai, T., Pollard, D.D., 2000b. Fracture spacing in layered rocks: a new explanation based on the stress transition. J. Struct. Geol. 22 (1), 43–57.

Biegel, R.L., Sammis, C.G., Dieterich, J.H., 1989. The frictional properties of a simulated gouge having a fractal particle distribution. J. Struct. Geol. 11 (7), 827–846.

Billi, A., 2005. Grain size distribution and thickness of breccia and gouge zones from thin (<1 m) strike-slip fault cores in limestone. J. Struct. Geol. 27 (10), 1823–1837.

Billi, A., Storti, F., 2004. Fractal distribution of particle size in carbonate cataclastic rocks from the core of a regional strike-slip fault zone. Tectonophysics 384 (1), 115–128.

Billi, A., Salvini, F., Storti, F., 2003. The damage zone-fault core transition in carbonate rocks: implications for fault growth, structure and permeability. J. Struct. Geol. 25 (11), 1779–1794.

Bjørk, T., 2006a. Quantification and modeling of deformation processes: motivated by observations from the contact to the Hornelen Basin, Bremangerland. Master's thesis, Physics of Geological Processes (PGP). Department of Physics, University of Oslo.

Bjørk, T., 2006b. Gray scale image analysis: image analysis program for use with matlab. http://folk.uio.no/torbjoeb/image_analysis/.

Bjørk, T., Mair, K., Austrheim, H., 2009. Quantifying granular material and deformation: advantages of combining grain size, shape, and mineral phase recognition analysis. J. Struct. Geol. 31 (7), 637–653.

Blenkinsop, T., 1991. Cataclasis and processes of particle size reduction. Pure Appl. Geophys. 136 (1), 59–86.

Blenkinsop, T., Fernandes, T., 2000. Fractal characterization of particle size distributions in chromitites from the Great Dyke, Zimbabwe. Pure Appl. Geophys. 157 (4), 505–522.

Buhl, E., Kowitz, A., Elbeshausen, D., Sommer, F., Dresen, G., Poelchau, M.H., Reimold, W.U., Schmitt, R.T., Kenkmann, T., 2013. Particle size distribution and strain rate attenuation in hypervelocity impact and shock recovery experiments. J. Struct. Geol. 56, 20–33.

Clark, C., Mumm, A.S., Collins, A.S., 2006. A coupled micro- and macrostructural approach to the analysis of fluid induced brecciation, Curnamona Province, South Australia. J. Struct. Geol. 28 (5), 745–761.

Cowan, D., 1999. Do faults preserve a record of seismic slip? A field geologist's opinion. J. Struct. Geol. 21, 995–1001.

Coward, M., 1980. Shear zones in the Precambrian crust of southern Africa. J. Struct. Geol. 2 (1), 19–27.

Delaney, P.T., Pollard, D.D., Ziony, J.I., McKee, E.H., 1986. Field relations between dikes and joints: emplacement processes and paleostress analysis. J. Geophys. Res., Solid Earth 91 (B5), 4920–4938.

Di Toro, G., Nielsen, S., Pennacchioni, G., 2005. Earthquake rupture dynamics frozen in exhumed ancient faults. Nature 436 (7053), 1009–1012.

Freund, L.B., 1990. Dynamic Fracture Mechanics. Cambridge University Press.

Glazner, A.F., Mills, R.D., 2012. Interpreting two-dimensional cuts through broken geologic objects: fractal and non-fractal size distributions. Geosphere 8 (4), 902–914.

Grady, D., Kipp, M., 1987. Dynamic rock fragmentation. In: Atkinson, B.K. (Ed.), Fracture Mechanics of Rock. Academic Press, London, pp. 429–475.

Griffith, W.A., Di Toro, G., Pennacchioni, G., Pollard, D.D., Nielsen, S., 2009a. Static stress drop associated with brittle slip events on exhumed faults. J. Geophys. Res., Solid Earth 114 (B2).

Griffith, W.A., Rosakis, A., Pollard, D.D., Ko, C.W., 2009b. Dynamic rupture experiments elucidate tensile crack development during propagating earthquake ruptures. Geology 37 (9), 795–798.

Griffith, W.A., Mitchell, T.M., Renner, J., Di Toro, G., 2012. Coseismic damage and softening of fault rocks at seismogenic depths. Earth Planet. Sci. Lett. 353, 219–230.

Gross, M.R., 1993. The origin and spacing of cross joints: examples from the Monterey Formation, Santa Barbara coastline, California. J. Struct. Geol. 15 (6), 737–751.

Hadizadeh, J., Johnson, W.K., 2003. Estimating local strain due to comminution in experimental cataclastic textures. J. Struct. Geol. 25 (11), 1973–1979.

Harris, R.A., Archuleta, R.J., Day, S.M., 1991. Fault steps and the dynamic rupture process: 2-D numerical simulations of a spontaneously propagating shear fracture. Geophys. Res. Lett. 18 (5), 893–896.

Hattori, I., Yamamoto, H., 1999. Rock fragmentation and particle size in crushed zones by faulting. J. Geol. 107 (2), 209–222.

Heilbronner, R., Keulen, N., 2006. Grain size and grain shape analysis of fault rocks. Tectonophysics 427 (1), 199–216.

Hobbs, B., Ord, A., Teyssier, C., 1986. Earthquakes in the ductile regime? Pure Appl. Geophys. 124 (1–2), 309–336.

Ide, S., Aochi, H., 2005. Earthquakes as multiscale dynamic ruptures with heterogeneous fracture surface energy. J. Geophys. Res. 110 (B11303).

Ide, S., Beroza, G.C., 2001. Does apparent stress vary with earthquake size? Geophys. Res. Lett. 28 (17), 3349–3352.

Isida, M., Noguchi, H., 1992. Stress intensity factors at tips of branched cracks under various loadings. Int. J. Fract. 54 (4), 293–316.

Jébrak, M., 1997. Hydrothermal breccias in vein-type ore deposits: a review of mechanisms, morphology and size distribution. Ore Geol. Rev. 12 (3), 111–134.

Joubert, P., 1974. Wrench-fault tectonics in the Namaqualand Metamorphic Complex. In: Contributions to the Precambrian Geology of Southern Africa. In: Chamb. Mines Precambr. Res. Unit Bull., vol. 15, pp. 17–26.

Kanamori, H., 1977. The energy release in great earthquakes. J. Geophys. Res. 82 (20), 2981–2987.

Kanamori, H., Brodsky, E.E., 2004. The physics of earthquakes. Rep. Prog. Phys. 67 (8), 1429.

Keulen, N., Heilbronner, R., Stünitz, H., Boullier, A.-M., Ito, H., 2007. Grain size distributions of fault rocks: a comparison between experimentally and naturally deformed granitoids. J. Struct. Geol. 29 (8), 1282–1300.

Kirkpatrick, J.D., Rowe, C.D., 2013. Disappearing ink: how pseudotachylytes are lost from the rock record. J. Struct. Geol. 52, 183–198.

Lachenbruch, A.H., Sass, J., 1977. Heat flow in the United States and the thermal regime of the crust. In: Geophys. Monogr., vol. 20, pp. 626–675.

Lambert, C., 2013. Granitic melt transport and emplacement along transcurrent shear zones: case study of the Pofadder Shear Zone in South Africa and Namibia. Master's thesis. Stellenbosch University, South Africa. 145 pp.

Lay, T., Wallace, T.C., 1995. Modern Global Seismology, vol. 58. Academic Press, New York.

Lin, A., 1996. Injection veins of crushing-originated pseudotachylyte and fault gouge formed during seismic faulting. Eng. Geol. 43 (2), 213–224.

Lin, A., 2011. Seismic slip recorded by fluidized ultracataclastic veins formed in a coseismic shear zone during the 2008 Mw 7.9 Wenchuan earthquake. Geology 39 (6), 547–550.

Lin, A., Fu, B., Guo, J., Zeng, Q., Dang, G., He, W., Zhao, Y., 2002. Co-seismic strike-slip and rupture length produced by the 2001 Ms 8.1 Central Kunlun earthquake. Science 296 (5575), 2015–2017.

Lin, S., Jiang, D., Williams, P.F., 2007. Importance of differentiating ductile slickenside striations from stretching lineations and variation of shear direction across a high-strain zone. J. Struct. Geol. 29 (5), 850–862.

Luther, A., Axen, G., Selverstone, J., 2013. Particle-size distributions of low-angle normal fault breccias: implications for slip mechanisms on weak faults. J. Struct. Geol. 55, 50–61.

MacClaren, A., 1988. The geology of the area east of Pofadder with emphasis on shearing associated with the Pofadder Lineament, Northwest Cape. Master's thesis. University of Cape Town.

Mandelbrot, B.B., 1982. The Fractal Geometry of Nature. Freeman and Co., New York.

Marone, C., Scholz, C., 1989. Particle-size distribution and microstructures within simulated fault gouge. J. Struct. Geol. 11 (7), 799–814.

Micklethwaite, S., Cox, S.F., 2004. Fault-segment rupture, aftershock-zone fluid flow, and mineralization. Geology 32 (9), 813–816.

Monzawa, N., Otsuki, K., 2003. Comminution and fluidization of granular fault materials: implications for fault slip behavior. Tectonophysics 367 (1), 127–143.

Ngo, D., Huang, Y., Rosakis, A., Griffith, W., Pollard, D., 2012. Off-fault tensile cracks: a link between geological fault observations, lab experiments, and dynamic rupture models. J. Geophys. Res., Solid Earth 117 (B1).

Okamoto, S., Kimura, G., Takizawa, S., Yamaguchi, H., et al., 2006. Earthquake fault rock indicating a coupled lubrication mechanism. eEarth Discuss. 1 (2), 135–149.

Passchier, C.W., Trouw, R.A., 2005. Microtectonics. Springer, New York.

Pavlis, T.L., Serpa, L.F., Keener, C., 1993. Role of seismogenic processes in fault-rock development: an example from death valley, California. Geology 21 (3), 267–270.

Pollard, D., Segall, P., 1987. Theoretical displacements and stresses near fractures in rock: with applications to faults, joints, veins, dikes, and solution surfaces. In: Fracture Mechanics of Rock, pp. 277–349.

Price, N.J., 1966. Fault and Joint Development in Brittle and Semi-Brittle Rock, vol. 1. Pergamon Press, Oxford.

Ravi-Chandar, K., Knauss, W., 1984. An experimental investigation into dynamic fracture: II microstructural aspects. Int. J. Fract. 26 (1), 65–80.

Reches, Z., Dewers, T.A., 2005. Gouge formation by dynamic pulverization during earthquake rupture. Earth Planet. Sci. Lett. 235 (1), 361–374.

Rice, J., 2006. Heating and weakening of faults during earthquake slip. J. Geophys. Res. 111, B05311.
Riley, P., Tikoff, B., 2010. Tabular fracture clusters: dynamic fracturing produced by volatile expulsion, Sierra Nevada Batholith, California. J. Struct. Geol. 32 (10), 1488–1499.
Rockwell, T., Sisk, M., Girty, G., Dor, O., Wechsler, N., Ben-Zion, Y., 2010. Chemical and physical characteristics of pulverized Tejon Lookout Granite adjacent to the San Andreas and Garlock faults: implications for earthquake physics. In: Mechanics, Structure and Evolution of Fault Zones. Springer, pp. 1725–1746.
Rosakis, A.J., 2002. Intersonic shear cracks and fault ruptures. Adv. Phys. 51 (4), 1189–1257.
Rosakis, A.J., Samudrala, O., Coker, D., 2000. Intersonic shear crack growth along weak planes. Mater. Res. Innov. 3 (4), 236–243.
Rowe, C., Kirkpatrick, J., Brodsky, E., 2012. Fault rock injections record paleoearthquakes. Earth Planet. Sci. Lett. 335, 154–166.
Sagy, A., Korngreen, D., 2012. Dynamic branched fractures in pulverized rocks from a deep borehole. Geology 40 (9), 799–802.
Sagy, A., Reches, Z., Roman, I., 2001. Dynamic fracturing: field and experimental observations. J. Struct. Geol. 23 (8), 1223–1239.
Sagy, A., Cohen, G., Reches, Z., Fineberg, J., 2006. Dynamic fracture of granular material under quasi-static loading. Geophys. Res. Lett. 111, B04406.
Sammis, C.G., Biegel, R.L., 1989. Fractals, fault-gouge, and friction. Pure Appl. Geophys. 131 (1–2), 255–271.
Sammis, C., King, G., Biegel, R., 1987. The kinematics of gouge deformation. Pure Appl. Geophys. 125 (5), 777–812.
Samudrala, O., Huang, Y., Rosakis, A., 2002. Subsonic and intersonic shear rupture of weak planes with a velocity weakening cohesive zone. J. Geophys. Res. 107 (B8), 2170.
Scholz, C., 1988. The brittle–plastic transition and the depth of seismic faulting. Geol. Rundsch. 77 (1), 319–328.
Scholz, C., 1998. Earthquakes and friction laws. Nature 391 (6662), 37–42.
Scholz, C., 2002. The Mechanics of Earthquakes and Faulting. Cambridge University Press, New York.
Sharon, E., Fineberg, J., 1996. Microbranching instability and the dynamic fracture of brittle materials. Phys. Rev. B 54 (10), 7128.
Sharon, E., Gross, S.P., Fineberg, J., 1996. Energy dissipation in dynamic fracture. Phys. Rev. Lett. 76 (12), 2117–2120.
Sibson, R., 1977. Fault rocks and fault mechanisms. J. Geol. Soc. 133 (3), 191–213.
Sibson, R., 1980. Transient discontinuities in ductile shear zones. J. Struct. Geol. 2 (1), 165–171.
Sibson, R., 1983. Continental fault structure and the shallow earthquake source. J. Geol. Soc. 140 (5), 741–767.
Sibson, R.H., 1984. Roughness at the base of the seismogenic zone: contributing factors. J. Geophys. Res., Solid Earth 89 (B7), 5791–5799.
Sibson, R., 1985. Stopping of earthquake ruptures at dilational fault jogs. Nature 316, 248–251.
Sibson, R., 1986. Brecciation processes in fault zones: inferences from earthquake rupturing. Pure Appl. Geophys. 124 (1), 159–175.
Sibson, R., 1989. Earthquake faulting as a structural process. J. Struct. Geol. 11 (1), 1–14.
Sibson, R., Moore, J., Rankin, A., 1975. Seismic pumping – a hydrothermal fluid transport mechanism. J. Geol. Soc. 131 (6), 653–659.
Stipp, M., Stünitz, H., Heilbronner, R., Schmid, S.M., 2002. The eastern Tonale fault zone: a natural laboratory for crystal plastic deformation of quartz over a temperature range from 250 to 700 °C. J. Struct. Geol. 24 (12), 1861–1884.
Stirling, M., Wesnousky, S., Shimazaki, K., 2007. Fault trace complexity, cumulative slip, and the shape of the magnitude–frequency distribution for strike-slip faults: a global survey. Geophys. J. Int. 124 (3), 833–868.
Storti, F., Billi, A., Salvini, F., 2003. Particle size distributions in natural carbonate fault rocks: insights for non-self-similar cataclasis. Earth Planet. Sci. Lett. 206 (1), 173–186.
Storti, F., Balsamo, F., Salvini, F., 2007. Particle shape evolution in natural carbonate granular wear material. Terra Nova 19 (5), 344–352.
Sylvester, A., 1988. Strike-slip faults. Geol. Soc. Am. Bull. 100 (11), 1666–1703.
Toogood, D.J., 1976. Structural and Metamorphic Evolution of a Gneiss Terrain in the Namaqua Belt Near Onseepkans, South West Africa. Chamb. Mines Precambr. Res. Unit Bull., vol. 19. University of Cape Town, Department of Geology.
Toy, V., Prior, D., Norris, R., 2008. Quartz fabrics in the Alpine Fault mylonites: influence of pre-existing preferred orientations on fabric development during progressive uplift. J. Struct. Geol. 30 (5), 602–621.
Tse, S., Rice, J., 1986. Crustal earthquake instability in relation to the depth variation of frictional slip properties. J. Geophys. Res. 91 (B9), 9452–9472.
Turcotte, D., 1986. Fractals and fragmentation. J. Geophys. Res., Solid Earth 91 (B2), 1921–1926.
USGS and Japan ASTER Program, 2013. ASTER scene AST_L1A_003_2123463321, 1A, USGS, Sioux Falls, 2013/3/20.
Valenta, R., Cartwright, I., Oliver, N., 1994. Structurally controlled fluid flow associated with breccia vein formation. J. Metamorph. Geol. 12 (2), 197–206.
Weatherley, D.K., Henley, R.W., 2013. Flash vaporization during earthquakes evidenced by gold deposits. Nat. Geosci. 6, 294–298.
White, J.C., 2012. Paradoxical pseudotachylyte–fault melt outside the seismogenic zone. J. Struct. Geol. 38, 11–20.
Wilson, B., Dewers, T., Reches, Z., Brune, J., 2005. Particle size and energetics of gouge from earthquake rupture zones. Nature 434 (7034), 749–752.
Wu, H., Pollard, D., 1995. An experimental study of the relationship between joint spacing and layer thickness. J. Struct. Geol. 17 (6), 887–905.
Xu, X.-P., Needleman, A., 1994. Numerical simulations of fast crack growth in brittle solids. J. Mech. Phys. Solids 42 (9), 1397–1434.